AD NUMBER

AD864561

LIMITATION CHANGES

TO:

Approved for public release; distribution is unlimited.

FROM:

Distribution authorized to U.S. Gov't. agencies only; Administrative/Operational Use; 16 JAN 1970. Other requests shall be referred to Office of Naval Research, Arlington, VA 20368.

AUTHORITY

ONR ltr 29 Aug 1973

PHILCO Ford

PHILCO-FORD CORPORATION
Aeronutronic Division
Newport Beach, California

Publication No. U4779

FINAL TECHNICAL REPORT II

QUANTUM INTERFEROMETER
ARPA Contract No. N00014-68-C-0138

Prepared by:
James E. Zimmerman
and Paul Thiene

Approved by:
Paul M. Sutton
Paul M. Sutton, Manager
Physics and Chemistry Laboratories

AERONUTRONIC DIVISION
PHILCO-FORD CORPORATION
NEWPORT BEACH, CALIFORNIA 92663

January 16, 1970

Sponsored by:
Advanced Research Projects Agency
ARPA Order No. 1049
Modification No. P001

BLANK PAGE

CONTENTS

CONTENTS (Continued)

ILLUSTRATIONS

ILLUSTRATIONS (Continued)

SUMMARY

A recapitulation of some of the work described in previous (quarterly) reports is given in this report. Stable rf-biased point-contact loop devices have been developed which are reliable under specified conditions of normal operational use. This seems to be a unique achievement, even though point-contact devices have been around for about six years already. High-frequency heterodyne detection with these devices has been studied in some depth, and a sensitivity of 10^{-16} watts per $\sqrt{hz}$ at 110 Mhz, with an intermediate frequency of 30 Mhz, was measured. A simple dc-biased point-contact device for millimeter-wave detection was invented and awaits further development.

Experimental magnetic detection systems have been built which demonstrate the practical possibility of achieving sensitivities of at least 10^{-9}-gauss field or 10^{-10}-gauss-per-cm gradient. Experiments with these systems have clearly established certain design principles which must be followed, and it is predicted that subsequent systems based on these principles will realize practical operational sensitivities at least an order of magnitude better than this. A compact portable magnetometer with $\sim 10^{-9}$-gauss sensitivity was used in a magnetically shielded facility

at the National Magnet Laboratory to measure the magnetic field of the human heart (magnetocardiogram) and it was shown that this method can now be seriously considered as a clinical and diagnostic technique. An ultra-sensitive gradiometer was operated in the open terrestrial environment, showing possibilities for geophysical prospecting and magnetic anomaly detection.

A mathematical analysis of certain modes of operation of quantum-interference devices is given which is useful in optimizing the circuit parameters required to match the devices to a load.

In the concluding remarks are listed a number of publications which have appeared or will appear soon on the work done under this contract. These publications contain a large amount of basic technical detail on what quantum interference devices are and how they work.

SECTION 1

RECAPITULATION OF WORK DESCRIBED IN DETAIL IN PREVIOUS QUARTERLY REPORTS

1.1 INTRODUCTION

This section is a summary review of some of the material that has been presented in detail in previous reports. We have particularly chosen to include material which relates to the main subject of this final report, namely, ultra-sensitive magnetometry with rf-biased point-contact quantum-interference devices (SQUIDs). Paragraphs 1.5 and 1.6 are a review of a study of devices for ultra-high-frequency detection.

1.2 QUANTUM INTERFERENCE MAGNETOMETRY AND THERMAL NOISE FROM A CONDUCTING ENVIRONMENT (Harding and Zimmerman, 1968)

We consider here the thermal noise contribution caused by the proximity of conducting bodies to a magnetometer. For this purpose the magnetometer is merely a loop which keeps track of its enclosed flux. The loop is a one degree of freedom system with a thermal energy 1/2 kT. It is important to note that the presence of a nearby conductor (with its thermal noise currents) cannot change the thermal energy of the loop; it can only modify the frequency distribution of that energy. The effect of

the conductor is to produce a frequency dependent inductance $L(\omega)$ and resistance $R(\omega)$ of the loop. Associated with the resistance is a Johnson noise source which generates a mean square voltage in the frequency interval $d\omega$, $V^2(\omega)d\omega = \frac{2}{\pi} kTR(\omega)d\omega$. We are interested in the magnetic flux produced in the loop. One might think that $\phi = LI$ where I is the current in the circuit. However, this is only the part of the flux in phase with I. The loop also senses the out-of-phase or dissipative component of the flux. In the absence of any d-c resistance in the circuit, the Johnson noise voltage is opposed only by the changing flux in the circuit. Hence $V^2(\omega) = \omega^2\phi^2(\omega)$ or

$$\phi^2(\omega)d\omega = \frac{2}{\pi} kTR(\omega)d\omega/\omega^2 \qquad (1\text{-}1)$$

$R(\omega)$ may be readily determined experimentally by measuring the frequency dependence of the complex impedance of the loop in the presence of the conductor (Zimmerman, 1961).

An alternative approach to the problem is to examine the normal modes of the cylinder and see how they couple to the detector. This approach was taken by Vant Hull, Simpkins, and Harding (1967) in explaining their experimental observations of magnetic fluctuations in conductors. The experiment consisted of placing a long conducting cylinder in the aperture of a quantum interference magnetometer. According to Van Hull, et al., the expected value of the axial component of the mean-square thermal fluctuation of magnetic flux in a cylinder is $\phi^2 = \mu_o kTA^2/V$ (MKS units), where A and V are the cross section and volume of the cylinder. This implies that ϕ^2 varies inversely with the sample length. This is at variance with equation (1-1) inasmuch as $R(\omega)$ clearly cannot depend on the length if it greatly exceeds the loop diameter. The implausibility of this predicted dependence on length has motivated us to look more carefully at the problem.

It was assumed by Vant Hull, et al., that only one mode, a uniform axial field, contributes to the flux seen by the detector. If the detector

were a long solenoid, this would be true. However a single turn coil is sensitive to a multitude of cylinder modes having axial current variation. It is in fact sensitive to all modes having an axial period greater than the diameter D of the detector loop; modes having a smaller period have a substantial fraction of their flux returning within the loop. The number of modes which contribute to the measured flux is of the order L/D, where L is the sample length. Each of these modes contributes approximately $\phi^2 = \mu_o kTA/D$. This result predicts an inverse dependence on the sensor diameter instead of the sample length. Since L/D was not varied by Vant Hull, et al., the effect of sample length, i.e., is unresolved experimentally. An exact analysis requires finding the normal modes in the conducting cylinder by solving the diffusion equation $\nabla^2 B = (\mu/\rho)\frac{\partial B}{\partial t}$ (a difficult problem). The amplitude of each mode is determined by setting the magnetic energy of the mode $\int \frac{B^2}{2\mu_o} dV$ equal to 1/2 kT. Integration of the field distribution over the sensor area yields the flux ϕ_i contributed by the ith mode. Associated with each mode is a characteristic relaxation or decay time τ. The mean square flux coupled by the sensor in the frequency interval $d\omega$ is given by Vant Hull, et al.,

$$\phi^2(\omega)d\omega = \sum_i \omega_i^2 \frac{2}{\pi} \frac{\tau_i \, d\omega}{I + \omega^2 \tau_i^2} \qquad (1\text{-}2)$$

This relation must of course give the same result as equation (1-1) and this has in fact been verified for the case of an infinite rod and solenoid for which $R(\omega)$ and τ are known (Zimmerman, 1961; Bean, de Blois, and Nesbitt, 1959). Equation (1-1) is useful in cases of complex geometries, for $R(\omega)$ can easily be measured as mentioned above. For a more general and practical discussion of thermal noise in magnetometry see Paragraph 2.2.

1.3 STABLE RF-BIASED POINT-CONTACT DEVICES (SQUIDS). (Zimmerman, Thiene, and Harding, 1970)

Several device configurations have been developed which have exhibited long-term reliability (that is, over a period of years), provided they are operated in a cryogenic system which does not allow atmospheric condensation on the device during warm up and cool down - a very easy requirement to satisfy.

Superconducting loop devices were made mechanically rugged to minimize the effects of mechanical vibration and shock, and were made entirely of one material to eliminate differential thermal expansion. The first such device to which these ideas were applied was made as shown in Figure 1-1. It consists essentially of a C-shaped niobium block, the jaws of the C being bridged by a small-area contact. The two opposing members of the contact are 000-120 niobium screws, one flat on the end, one pointed, and the screws are positioned as close to the center hole as possible to minimize the effect of vibration. The point was formed on a jeweler's lathe and was honed to microscopic sharpness.

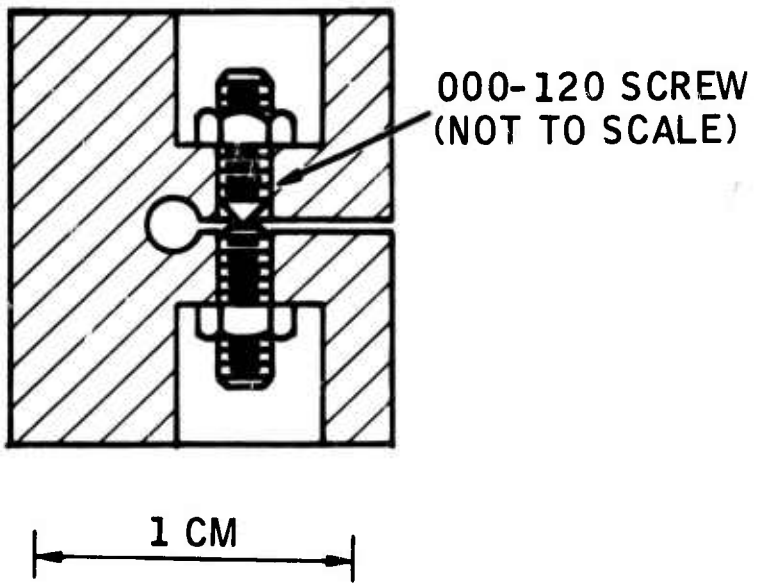

FIGURE 1-1. STABLE SUPERCONDUCTING POINT-CONTACT LOOP DEVICE

The C-shaped structure is susceptible to severe mechanical or thermal shock. A much more rugged device is the symmetric structure shown in Figure 1-2. Owing to is particular geometry and topology, it differs from the previous device in its response to applied time-varying magnetic fields. The total flux within the two holes of the device is constant in time ("trapped") and is not a function of applied field. The quantum interference phenomenon is observed by modulating flux from one hole to the other, which is accomplished by means of a coil inserted in one or the other of the two holes, or by applying the appropriate component of field gradient to the device. If the trapped flux in the device is non-zero, inserting a magnetic material in one hole will also shift flux from one hole to the other, so the device is useful as a self-contained susceptibility bridge. A uniform applied field gives no shift or change of flux, and hence no response. To use it as a magnetometer requires a superconducting "flux transformer." The use of this device as a detector element, in conjunction with a flux transformer as a coupling element to the external field, permits great flexibility in design and application.

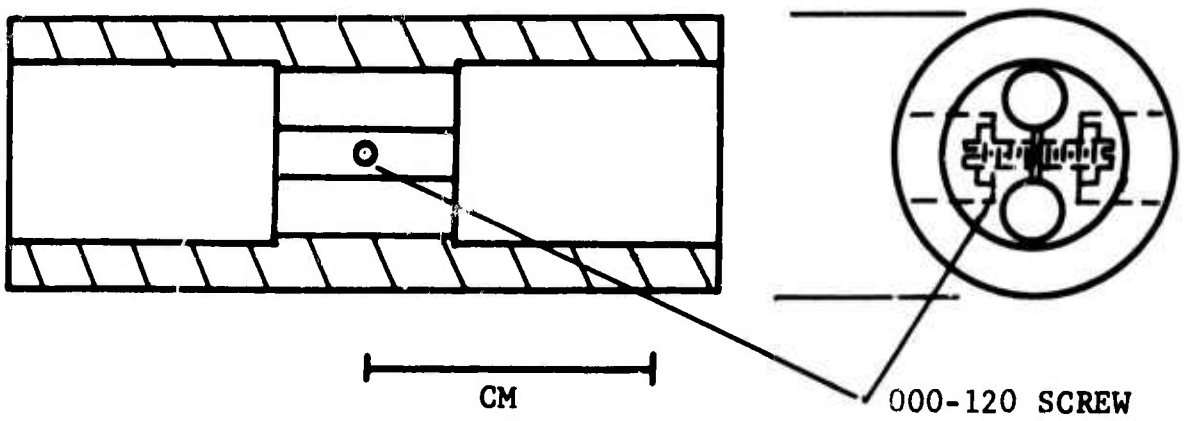

FIGURE 1-2. THE SYMMETRIC DEVICE

It might be pointed out in passing that the symmetric structure is particularly convenient for microwave detection or mixing experiments. The two holes connected by a narrow slot form a capacitively-loaded waveguide with a cutoff wavelength of a cm or more depending on the slot width. Microwave radiation from a rectangular waveguide can therefore be fed into the end of the device through a transition section or funnel, to travel down the slot and impinge on the contact. The dominant mode of propagation is also the one giving maximum coupling to the current through the contact.

Construction of resistive devices involves the use of two different materials, and so differential expansion is a serious problem. A design which in principle compensates for the effects of differential expansion is shown in Figure 1-3. By dividing the resistive section into two identical parts, symmetrically arranged, the thermal expansion integral around the loop vanishes to a first approximation. Several such devices were constructed. The resistive material was copper with up to 10 atomic percent germanium to increase the resistivity. The resistive alloy was bonded to the niobium by induction melting it in a pure helium atmosphere. One technique was to mill a slot in a block of niobium, place a

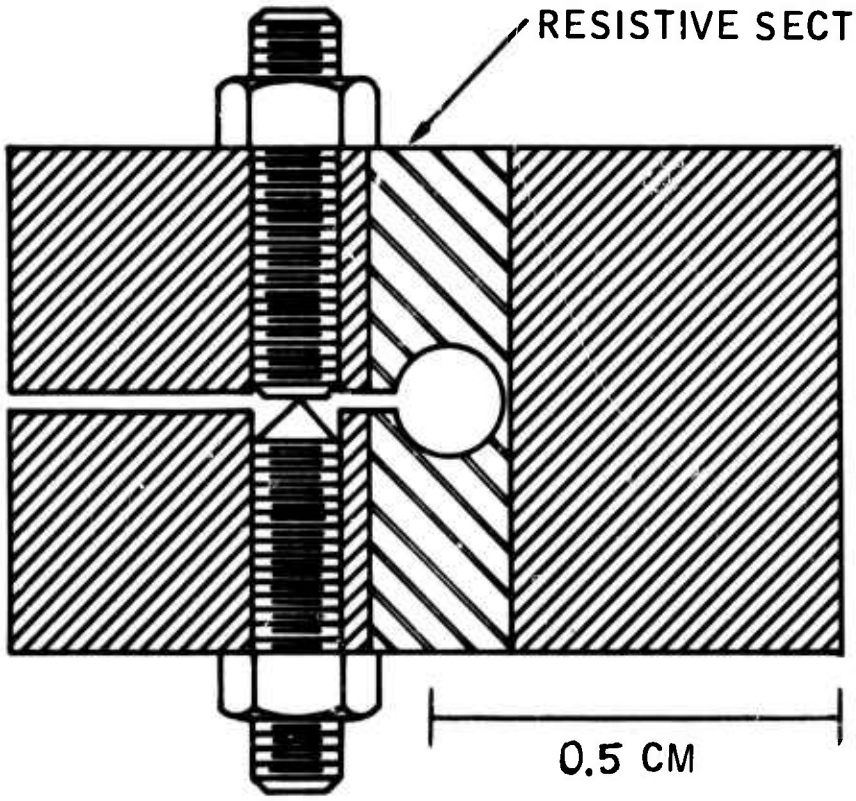

FIGURE 1-3. TEMPERATURE-COMPENSATED RESISTIVE-LOOP DEVICE

slab of the alloy in the slot, and then heat the block to a temperature well above the melting point of the alloy. Very good, bubble-free bonds were obtained if the helium atmosphere was sufficiently pure and the metal parts were well cleaned. The device was machined from the composite block. So far as long-term reliability is concerned, this design was only marginally successful. A device with a 0.15-mm thick resistive section was temperature cycled 14 times in 45 days with no appreciable change of characteristics, but several devices with 1.5-mm thick resistive sections survived no more than a few temperature cycles, the contact generally getting weaker with each cycle.

With all of these devices, the contact was adjusted one time only, at room temperature, except when they were exposed to atmospheric condensation. Under the latter condition a device would usually require readjusting after 10 or more warmup cycles. Most of the experiments discussed in Section 2 were done with the symmetric type of device, but part of the work in magnetocardiography was done with a C-shaped device which had been enclosed and used in a sealed probe since January 1968.

The partly-resistive loop device has a number of interesting applications which have been discussed in the literature (Zimmerman, Cowan, and Silver 1966; Kamper 1966; Silver, Zimmerman, and Kamper 1967; Zimmerman and Silver 1968). See also Paragraph 1.5.

An important point which has often been omitted from technical reports and publications on this subject is that these devices operate at the convenient temperature of 4.2°K, that is, at the normal boiling point of liquid helium, and that the operating temperature is not extremely critical.

1.4 DETAILED DESCRIPTION OF THE OPERATION OF RF-BIASED DEVICES

Superconducting point-contact loop devices exhibit a set of quantized fluxoid states spaced by the flux quantum $\varphi_o = 2e/h$. Under the application of a small rf-bias field, the flux through the loop is modulated by

the rf field. The amplitude of the modulation is small if the rf field is centered on a fluxoid state (dc field = n φ_o), since the loop remains in that state, and is large if the rf field is centered halfway between two fluxoid states (dc field = (n + 1/2)φ_o), since the loop switches between the two neighboring states at the radio frequency ω. Hence the rf voltage across a coil of N turns coupled to the loop varies between $\sim$ 0 and $\sim N\varphi_o\omega$ as the dc field is changed from an integral to a half-integral multiple of the flux quantum.

It is this periodic variation of rf impedance with dc (or low-frequency) fields which is the basis of the use of a SQUID in ultra-sensitive magnetometry.

The behavior of the devices with rf bias has been described in considerable detail by Silver and Zimmerman, 1967 and by Zimmerman, Thiene and Harding, 1970.

1.5 HETERODYNE DETECTION WITH SUPERCONDUCTING POINT CONTACTS AND ENHANCED HETERODYNE SIGNALS FROM TIGHTLY-COUPLED CONTACTS (Zimmerman, 1970)

Several modes of operation of point contact loop devices as heterodyne detectors in the frequency range 0 to 10^{10} hz were investigated experimentally. A point contact in a superconducting loop, under the application of two externally-generated a-c fields, behaved as expected on the basis of previous work (Silver and Zimmerman, 1967). Likewise, a point contact in a partly-resistive loop, in which an externally-generated signal is heterodyned with the Josephson oscillation of the contact, gave the expected results. In these modes of operation a sensitivity of 10^{-16} watts per $\sqrt{\text{hz}}$ at 110 Mhz, using an intermediate frequency of 30 Mhz, was indicated. On the other hand, an anomalously large heterodyne signal was obtained from a pair of closely-coupled Josephson-oscillating contacts. No explanation of this result is offered, but it appears that a sort of amplification of the heterodyne signal is effected when the Josephson frequencies are larger than the heterodyne frequency.

1.6 A SIMPLE DC-BIASED DEVICE FOR MILLIMETER-WAVE DETECTION

A closely-spaced pair of circular flat metal discs has a set of microwave resonances which can be excited by the Josephson oscillation of a dc-biased superconducting point-contact bridging the gap at the center of the discs. The energy absorbed by these resonances is seen as a step or perturbation in the IV characteristic of the contact, at voltages given by the Josephson frequency relation $V_i = \varphi_o f_i$, where f_i is the frequency of the ith mode. The highest observed step corresponded to a frequency of about 150×10^9 hz, or 2 mm wavelength. This has been called self-detection of Josephson radiation (Dayem and Grimes, 1966; Eck, Scalapino, and Taylor, 1965). Similarly, if external microwave radiation is coupled into the parallel-disc cavity at one of the frequencies f_i, the width of the step at V_i will be increased, so that the configuration is useful as a microwave detector. This application has not been followed up; however, it is suggested that the configuration has some important attributes of a practical device, namely, simplicity and ruggedness. Since it seems straightforward to couple microwave power into the cavity efficiently, it would be interesting to evaluate the device as a millimeter-wave detector.

SECTION 2

DESIGN AND APPLICATIONS OF PORTABLE MAGNETOMETERS AND MAGNETIC GRADIOMETERS USING SUPERCONDUCTING TRANSFORMERS AND QUANTUM FLUX SENSORS

2.1 INTRODUCTION

This section describes some of the design principles of magnetometers utilizing superconducting quantum devices as flux sensors and using superconducting transformers to couple the device to the field being measured, and presents some experimental results.

A schematic of a flux transformer and a device is given in Figure 2-1. The flux transformer is topologically a closed loop, shown here as an external coil L_1 coupled to a magnetic field B and connected to a coil L_2 which is tightly coupled to the superconducting quantum interference device or SQUID. Because of the close coupling, the mutual inductance M will be nearly equal to, but less than, $\sqrt{L_2 L.}$ Two configurations are shown in Figure 2-1. On the left, L_1 is a uniform coil, and application of a field B causes a current to flow in the topological loop formed by L_1 and L_2. On the right, L_1 is shown as two equal coils in series opposition, so that there is no response to a uniform applied field, but a current will be induced proportional to the gradient of the field in neighborhood of the two coils.

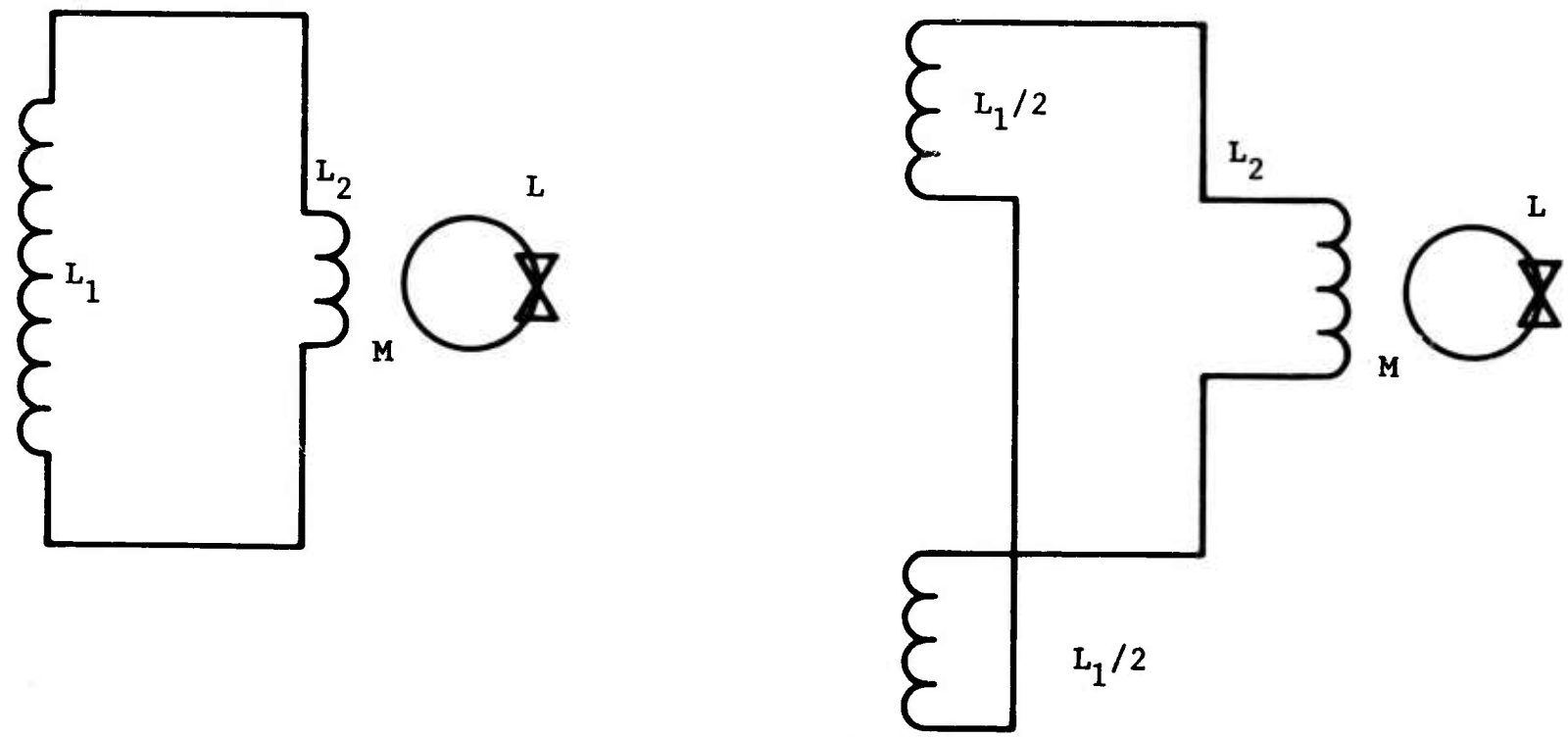

FIGURE 2-1. SCHEMATIC OF FLUX TRANSFORMERS: FIELD-SENSITIVE AND GRADIENT-SENSITIVE CONFIGURATIONS

BLANK PAGE

Different transformer configurations can be devised which will couple the device to any component of the field or its derivatives. We will restrict our attention to the field and its first derivative or gradient. The field B has three components (B_x, B_y and B_z). The gradient is a symmetric second-rank tensor (components $\partial B_x/\partial_x$, $\partial B_x/\partial_y$, etc.) with five independent components, since curl B = 0 and div B = 0 for static fields in empty space. Thus there is a total of eight independent quantities to be measured in order to specify the field and the gradient at any point in space. We will not speculate on how all this information might be used in practice, but we will discuss briefly the relative merits of field measurements compared to gradient measurements for airborne magnetic anomaly detection. In this application one flies a magnetometer over an area and obtains a magnetic map of the area. If the field components are mapped, then the gradient components can be derived or vice versa.

The advantage of gradient, as compared to field measurements, lies in its discrimination against the effect of temporal variation. To take a very simple model, consider a spatially uniform but time-varying background field $B_o(t)$, upon which is superimposed a small anomaly $B_a(x,y,z)$ such as might be produced by a localized lump of paramagnetic material. If, in scanning the magnetic field in the neighborhood, the variation of $B_o(t)$ during the time τ required to fly through the neighborhood of the anomaly is large compared to the anomaly itself, then there is absolutely no way of recognizing that an anomaly exists. On the other hand, gradient measurements through the same region will give a zero result everywhere except in the neighborhood of the anomaly, so that the anomaly is certain to be recognized regardless of the temporal variations of the background field, provided the gradiometer has sufficient sensitivity.

The fundamental disadvantage of a gradient-measuring (as compared to a field-measuring) instrument for terrestrial magnetic-anomaly detection

is the requirement for relatively enormous sensitivity. A gradiometer is nothing more than a magnetometer in a configuration such that the response is proportional to the change of field δB between two points separated by a distance ℓ, which will be called the gradiometer baseline. Thus, the gradient G is

$$G = \Delta B/\ell . \tag{2-1}$$

A straightforward way to measure gradients is to carry two magnetometers separated by a distance ℓ. In geophysical prospecting this has been done by carrying one magnetometer in an aircraft and suspending the other one a hundred feet or so beneath the aircraft with a cable. As the above equation indicates, the minimum detectable gradient should vary inversely with ℓ. However, there are limits on how large the baseline can be made, and furthermore, as is made large, it becomes difficult to maintain precise spacing and orientation of one magnetometer relative to the other. In any case, for reasonable values of ℓ, we shall assume that

$$\ell \ll d, \tag{2-2}$$

where d is the distance from the gradiometer to the source of the anomaly. Under this condition it is easy to show that

$$\Delta B \ll B, \tag{2-3}$$

so a magnetometer sufficiently sensitive to detect B at a distance d from the source may be not nearly sensitive enough to detect the change ΔB over a baseline ℓ.

In addition to ℓ and d, there is a third dimension or set of dimensions pertinent to the problem of magnetic-anomaly detection, namely, the size of the source. For simplicity we will assume that the source has a single characteristic dimension ℓ', which may be small compared with d in some applications such as submarine detection with airborne instruments, or large compared with d as in geophysical prospecting. The latter

case is outside the scope of this report. We will consider only the case

$$\ell' \ll d, \tag{2-4}$$

so that the source can be approximated by a dipole. The radial and transverse field components are

$$B_r = \frac{p \cos \theta}{2\pi d^3} \tag{2-5}$$

and

$$B_\theta = \frac{p \sin \theta}{4\pi d^3},$$

where p is the dipole moment and θ is the angular displacement of the test position from the dipole axis.

The field gradient as noted above has nine components

$$\begin{pmatrix} \frac{\partial B_x}{\partial x} & \frac{\partial B_x}{\partial y} & \frac{\partial B_x}{\partial z} \\ \frac{\partial B_y}{\partial x} & \frac{\partial B_y}{\partial y} & \frac{\partial B_y}{\partial z} \\ \frac{\partial B_z}{\partial x} & \frac{\partial B_z}{\partial y} & \frac{\partial B_z}{\partial z} \end{pmatrix}, \tag{2-6}$$

which with curl B = div B = 0 reduces to five. If we think of a magnetometer as an instrument which measures the flux through a loop, then a gradiometer can be constructed by using two such loops in series separated by the baseline ℓ. The two loops can be either coaxial or coplanar. The coaxial configuration measures a diagonal component of the gradient, depending upon its orientation. The coplanar configuration measures an off-diagonal component (see Figure 2-2). We are not aware of any compelling reasons why any particular component or components of the gradient would be most effective to measure for magnetic anomaly detection. Probably it would make little difference, since all the components are of

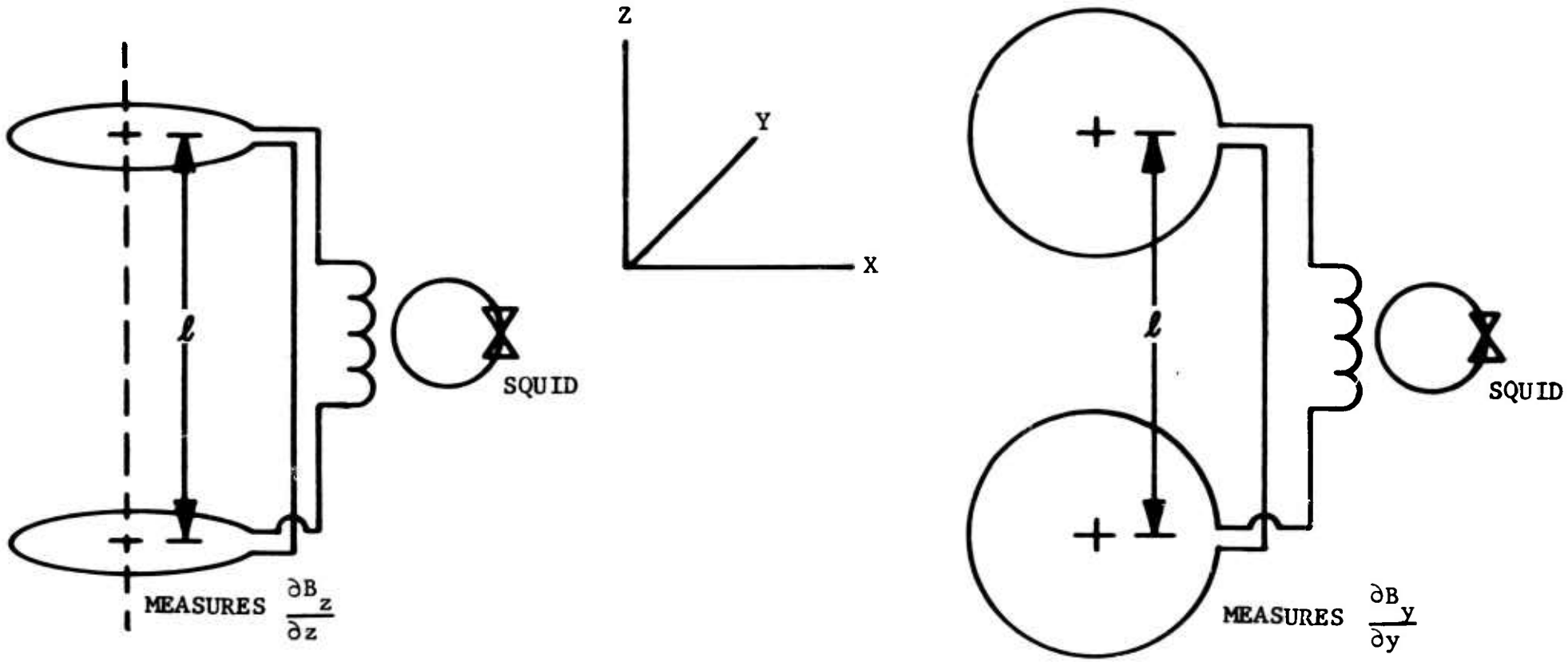

FIGURE 2-2. GRADIENT-SENSITIVE CONFIGURATIONS: DIAGONAL AND OFF-DIAGONAL ALIGNMENT

comparable magnitude except in certain positions such as along the dipole axis. For reasons of experimental simplicity in this preliminary study, we have used the coaxial configuration in the vertical orientation so that we measure $\partial B_z/\partial z$. Our purpose was to study the design problems involved in the construction of a gradiometer using a superconducting quantum device (SQUID) as a flux sensor and a superconducting flux transformer as a coupling element between the field and the sensor, and to attempt to achieve the ultimate level of sensitivity of which these devices are inherently capable.

2.2 INHERENT SENSITIVITY OF A SQUID - INTRINSIC AND EXTRINSIC THERMAL NOISE

We consider three noise sources which might contribute to the ultimate sensitivity of the SQUID as a flux detector. These are (1) "intrinsic" noise produced by thermal fluctuations of the normal electrons in the SQUID itself, (2) thermal-fluctuation noise from normal metal parts in the neighborhood of the SQUID or flux transformer, such as a room-temperature aluminum cylinder enclosing the cryostat, and (3) noise generated in the preamplifier input.

Thermal fluctuations of the normal electrons in the SQUID at temperature T produce a Johnson noise emf, given by

$$\frac{\overline{dV_n^2}}{d\omega} = (2/\pi)kTR\,, \tag{2-7}$$

where k is Boltzmann's constant and R is the normal resistance of the point contact. In the absence of any supercurrent, this produces a flux fluctuation spectrum in the SQUID given by

$$\frac{\overline{d\varphi_n^2}}{d\omega} = \frac{(2/\pi)\ L^2kTR}{R^2 + \omega^2L^2}\,. \tag{2-8}$$

BLANK PAGE

The integral of this gives the total fluctuation

$$\overline{\varphi_n^2} = LkT. \tag{2-9}$$

The spectrum is plotted in Figure 2-3. It is maximum at zero frequency and drops to one-half at $\omega = R/L$. The zero-frequency value can be written

$$\frac{1}{\varphi_o^2}\left(\frac{d\overline{\varphi_n^2}}{d\omega}\right) = \frac{2\ LkT}{\pi\varphi_o^2}\ (L/R) \sim 10^{-2}\ L/R\ . \tag{2-10}$$

The numerical value is calculated for a typical SQUID ($L \sim 10^{-9}$ h) at 4.2 degrees. The value of R can only be guessed at; it is probably of the order of 10 ohms, so the rms flux fluctuation per unit bandwidth in the neighborhood of zero frequency is

$$\left(\frac{d\overline{\varphi_n^2}}{d\omega}\right)^{\frac{1}{2}}\Bigg|_{\text{intrinsic}} \sim 10^{-6}\ \varphi_o\ \text{sec}^{\frac{1}{2}}\ . \tag{2-11}$$

The flux-fluctuation spectrum produced by a ring or cylinder of normal metal is calculated in exactly the same way as above, where L and R are replaced by the values of inductance and resistance, L_{cyl} and R_{cyl}, for the normal metal ring. A cylindrical normal-metal rf shield enclosing the SQUID and flux transformer is an example. Typically the decay time L_c/R_c for such an enclosure might be 10^{-4} sec or more, so the low-frequency ($\omega \ll R_c/L_c$) spectral intensity is

$$\left(\frac{d\overline{\varphi_n^2}}{d\omega}\right)^{\frac{1}{2}}\Bigg|_{\text{external}} \begin{cases} \sim 10^{-2}\ k\varphi_o\ \text{sec}^{\frac{1}{2}} \text{ for } T = 300 \text{ deg} \\ \sim 10^{-3}\ k\varphi_o\ \text{sec}^{\frac{1}{2}} \text{ for } T = 4.2 \text{ deg}, \end{cases} \tag{2-12}$$

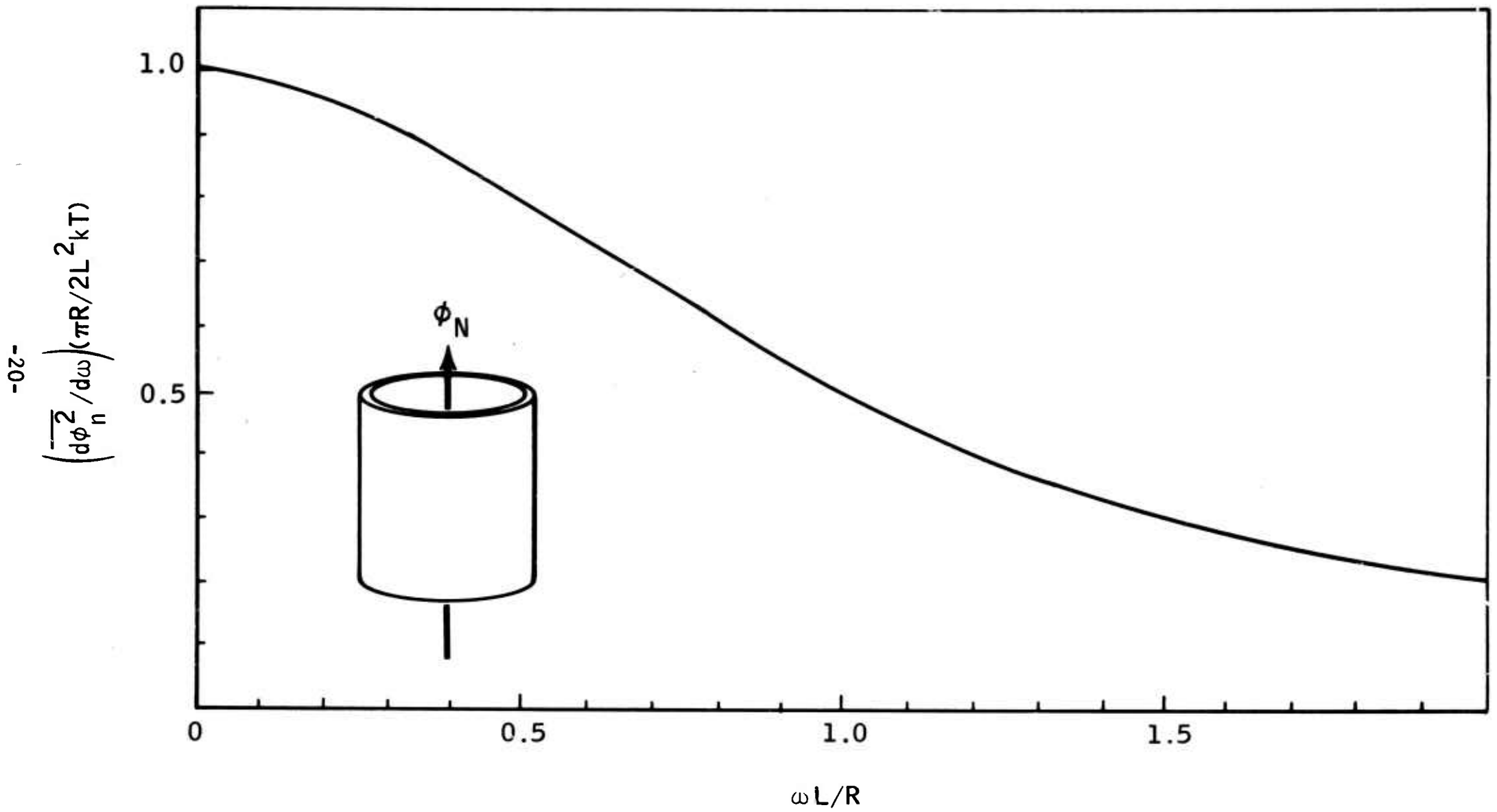

FIGURE 2-3. FLUX-FLUCTUATION SPECTRUM IN A CONDUCTING LOOP IN THERMAL EQUILIBRIUM

where k is the coupling coefficient between the shield and the SQUID. Here it is envisioned that the rf shield might enclose the whole cryostat, or might sit inside the helium bath in much closer proximity to the SQUID and flux transformer. In the first case the flux fluctuation is much greater, but on the other hand a smaller fraction of the fluctuation is seen by the flux transformer, owing to the lower coupling.

The fluctuation mode considered above is just one of an infinity of "decay modes" of the normal metal cylinder. These modes are solutions of the diffusion equation for the particular geometry of the normal conductor, the nth mode being characterized by a time constant τ_n and embodying an average magnetic energy of 1/2 kT. For the lowest decay mode of the cylinder, $\tau_1 = L_{cyl}/R_{cyl}$. Thus the fluctuation spectrum cannot in general be characterized by a single time constant, since all of the modes of the system, both intrinsic and extrinsic, will contribute. Regardless of the spectral distribution, however, the total thermal magnetic energy in the SQUID is just 1/2 kT, since the SQUID is a one degree of freedom system (Harding and Zimmerman, 1968). The presence of normal metal (at temperature T) in the neighborhood of the SQUID can only modify the spectral distribution but not the total magnitude of the thermal magnetic energy.* Furthermore, for a cylindrical normal-metal enclosure surrounding the SQUID the major contribution will be from the lowest decay mode, so that to good approximation the low-frequency fluctuation spectrum will be of the form given in Figure 2-3, characterized by the decay time L_{cyl}/R_{cyl}.

Now consider noise generated in the rf amplifier input. Experimentally we have shown (Zimmerman, Thiene, and Harding 1970) that the fluctuation level at the output of the SQUID electronics is equivalent to a spectral intensity of $1.6 \times 10^{-4}\, \varphi_o\, \text{sec}^{\frac{1}{2}}$ in the neighborhood of zero

---

*Whether the SQUID "sees" the normal metal enclosure directly or is coupled to it through the flux transformer does not alter this conclusion.

frequency, with the SQUID enclosed in a superconducting shield. This is considerably larger than the estimated intrinsic level given in Eq. 2-11 above ($\sim 10^{-6}\ \varphi_o\ \sec^{\frac{1}{2}}$), and indicates that the observed noise level can be ascribed primarily to fluctuations at the preamplifier input; that is

$$\left(\frac{\overline{d\varphi_n^2}}{d\omega}\right)^{\frac{1}{2}}\Bigg|_{\text{preamp}} \sim 10^{-4}\ \varphi_o\ \sec^{\frac{1}{2}}. \qquad (2\text{-}13)$$

If the SQUID is tightly coupled to a rod or cylinder of normal metal at the same temperature, then the spectral intensity may be $10^{-3}\ \varphi_o\ \sec^{\frac{1}{2}}$ or greater depending upon the time constants of the dominant decay modes. This level is greater than either the intrinsic contribution or the preamplifier contribution, and so is easily observable (Silver, Zimmerman, and Kamper, 1967); (Vant-Hull, Simpkins, and Harding, 1967).

2.3 EFFECT OF INTERFERENCE ON SQUID OPERATION; RF SHIELDING AND DYNAMIC RANGE

The very broad frequency response and high sensitivity of superconducting quantum devices has been widely remarked, especially in promotional-type presentations. In fact this property is a mixed blessing, since at the same time the dynamic range of the devices is very small compared to that of many electronic devices. If the total of all extraneous signals, thermal noise as well as interference such as local radio and radar stations and ignition noise, over the frequency range 0 to 10^{12} hz, has an rms magnitude of the order of $\varphi_o/2$ or greater in the SQUID, then the quantum periodic response is smeared over half a period or more. This means, in effect, that the SQUID has been wiped out as a useful device. The full implications of this limitation on dynamic range will be appreciated if it is recalled that helium-temperature thermal noise alone gives a fluctuation of the order of $0.1\ \varphi_o$ (Eq. 9, with $L \sim 10^{-9}$ h and $T \sim 4$ deg).

This discussion makes it clear that a SQUID magnetometer must be enclosed in a shield so that the SQUID is not exposed to the full spectrum of terrestrial interference.

In the preceding section it was pointed out that a metallic shield tends to increase the thermal fluctuation spectral intensity in the region of zero frequency, that is, in the very region that is of interest in magnetometry. The increase is enhanced if the shield is of high-conductivity and is closely-fitted around the SQUID and flux transformer.

The gist of the matter is that a shielding enclosure is essential to keep the SQUID within its dynamic range, but the shield can only degrade the magnetometer sensitivity by increasing the low-frequency spectral intensity of thermal noise. Thus the design of an optimum shield is much more subtle than one might naively suppose. It involves considerations of size, geometry, terrestrial noise spectrum, magnetometer bandwidth and application, and so on. For present purposes we will note merely that the shield should have as low conductivity as possible consistent with the requirement of keeping interference to an acceptable level, and if the shield is at room temperature it should be as large as possible consistent with requirements of portability and the like.

Another essential consideration in shield design, unrelated to the above, is discussed in the next section.

2.4 MAGNETOSTATIC AND GEOMETRIC PRINCIPLES OF FLUX-TRANSFORMER DESIGN

In the Seventh Quarterly Report, we presented some theorems on flux transformers, namely:

> Th. (1): For a given external coil inductance L_1, the greatest response is achieved if the internal coil has the same inductance, that is, if $L_2 = L_1$.

Th. (2): Under this condition, the flux in the SQUID is determined by the condition that the field energy in the SQUID is 1/4 the short-circuit free energy of the external coil in the applied field B. Thus

$$\frac{1}{2}\frac{\varphi_s^2}{L} \leq \frac{1}{4}\left(\frac{1}{2}\frac{\varphi_x^2 N_1^2}{L_1}\right), \quad \text{or} \quad \varphi_s \leq \frac{1}{2}\frac{\varphi_x}{L_1^{\frac{1}{2}}}\frac{N_1 L^{\frac{1}{2}}}{} = \frac{1}{2}\frac{N_1 B A_1}{L_1/L} \tag{2-14}$$

$$B_x \cong 2\,\varphi_s \sqrt{L_1/L}\,/A_1 N_1 \cong 2\,B_s \sqrt{V/V_1} \tag{2-15}$$

$$\varphi_s \cong 2\,\varphi_s \sqrt{\frac{A_1 \ell}{\ell_1 A}} \tag{2-16}$$

where φ_s is the flux in the SQUID, φ_x is the applied flux within the projected area A_1 of the external coil due to the field B_x, and N_1 and L_1 are respectively the number of turns and the inductance of the external coil. V, A, and ℓ are respectively the internal volume, area, and length of the SQUID, $L \cong \mu_o A/\ell$, $L_1 \cong \mu_o A_1/\ell_1$, , and $B_s = \varphi_s/A$.

Th. (3): If we assume for simplicity that L_1 is a single-layer coil of given ℓ_1 and area A_1, then L_1 is proportional to N_1^2. Therefore, the optimum response $\varphi_{s_{max}}$ is independent of N_1, and is proportional to the square root of the volume of the external coil (substitute $L_1 \propto N_1^2 A_1/\ell_1$ in Eq. 2-14).

Theorem (1) above defines the condition for achieving maximum flux in the SQUID, namely, $L_2 = L_1$. As a matter of fact, this is not quite the condition for maximum signal-to-noise. It has been pointed out several times (Quarterly Reports #1 and #7) that the signal-to-noise ratio of an rf-biased SQUID is enhanced by the presence of the flux transformer, owing to the reduction of SQUID effective inductance. Denoting this by L_{eff}, we have

$$L_{eff} = L - \frac{M^2}{L_1 + L_2} \tag{2-17}$$

If we replace L in Eq. 2-9 with L_{eff}, and then maximize the signal-to-noise ratio φ_s^2/φ_n^2, we get the condition

$$L_2/L_1 = (1 - k^2)^{-\frac{1}{2}} \tag{2-18}$$

where $k^2 = M^2/\sqrt{LL_2}$ is the coupling coefficient. With point-contact SQUIDs it is difficult to achieve k greater than about 0.8. For this value of k we have $L_2/L_1 = 5/3$, which is not grossly different from the condition for maximum flux ($L_2 = L_1$).

In designing an instrument to measure a component of the field gradient, and not to respond to any component of the field itself, it is essential to recognize an important geometric requirement, namely, that the entire apparatus possesses a high degree of symmetry, such as two-fold rotational symmetry about an axis and mirror symmetry about a plane perpendicular to that axis. We emphasize this requirement because, had we recognized it initially rather than discovering it operationally, the work reported herein would have proceeded much more rapidly.

Any piece of superconducting metal has an induced dipole moment proportional to the ambient magnetic field. If the piece of metal is off-center, then in general the dipole field will be different at opposite ends of the gradiometer baseline. Thus the gradiometer can "see" a uniform applied field through the coupling provided by the induced dipole field.

Similarly, any piece of normal metal has an induced eddy-current dipole moment in a fluctuating uniform field. If it is located asymmetrically, then it will couple the gradiometer to the ac components of the uniform field. For this reason, all metal parts of the apparatus, and especially the rf shield surrounding the gradiometer, should satisfy the minimum symmetry requirement. (Although symmetry provides a convenient way of getting null response to uniform field, it is not necessary per se. For example, in the coaxial loop arrangement of Figure 2-1,

an induced dipole located anywhere on, and oriented perpendicular to, any meridian plane has no effect. With the coplanar loops, any dipole lying with its axis in the plane of the loops has no effect. Also for example, the two loops need not be geometrically identical, but must have equal effective areas.)

Unavoidably, or for convenience in construction, there will be small deviations from symmetry in any practical design. Compensating controls are therefore required to null out the effect of the residual asymmetry. It is anticipated that fluctuations in the earth's field may amount to 10^{-5} gauss or more in one second. If we expect to measure field gradients of the order of 10^{-10} gauss over the gradiometer baseline, then it is necessary that the gradiometer be balanced to one part in 10^5 or better. With proper design, the residual asymmetry should be as little as one part in 10^3, so that compensation to one percent of the residual will achieve the desired balance and make the gradiometer insensitive to uniform field fluctuations.

2.5 AN EXPERIMENTAL TERRESTRIAL GRADIOMETER

During the last six months a series of field tests on an ultra-sensitive gradiometer were carried out, during which the instrument evolved through several major design modifications. The heart of the first model is shown in Figure 2-4. (This was Figure 9 in the Fifth Quarterly Technical Report, No. U4604). These components were mounted together as a rigid unit, using non-metallic hardware (micarta sheet, nylon screws, etc.) in a glass helium Dewar of about two-liter capacity, inside a glass nitrogen Dewar. The entire cryostat was mounted inside a cylindrical aluminum shield with closed ends as sketched in Figure 2-5. Essentially complete closure of the shield was necessary in field operation to prevent swamping the SQUID with radio and radar interference. A miniaturized, battery-operated electronic package was mounted on top of the aluminum shield at the upper end of the "coax to preamp" indicated in Figure 2-4. The electronic package contained the units shown in

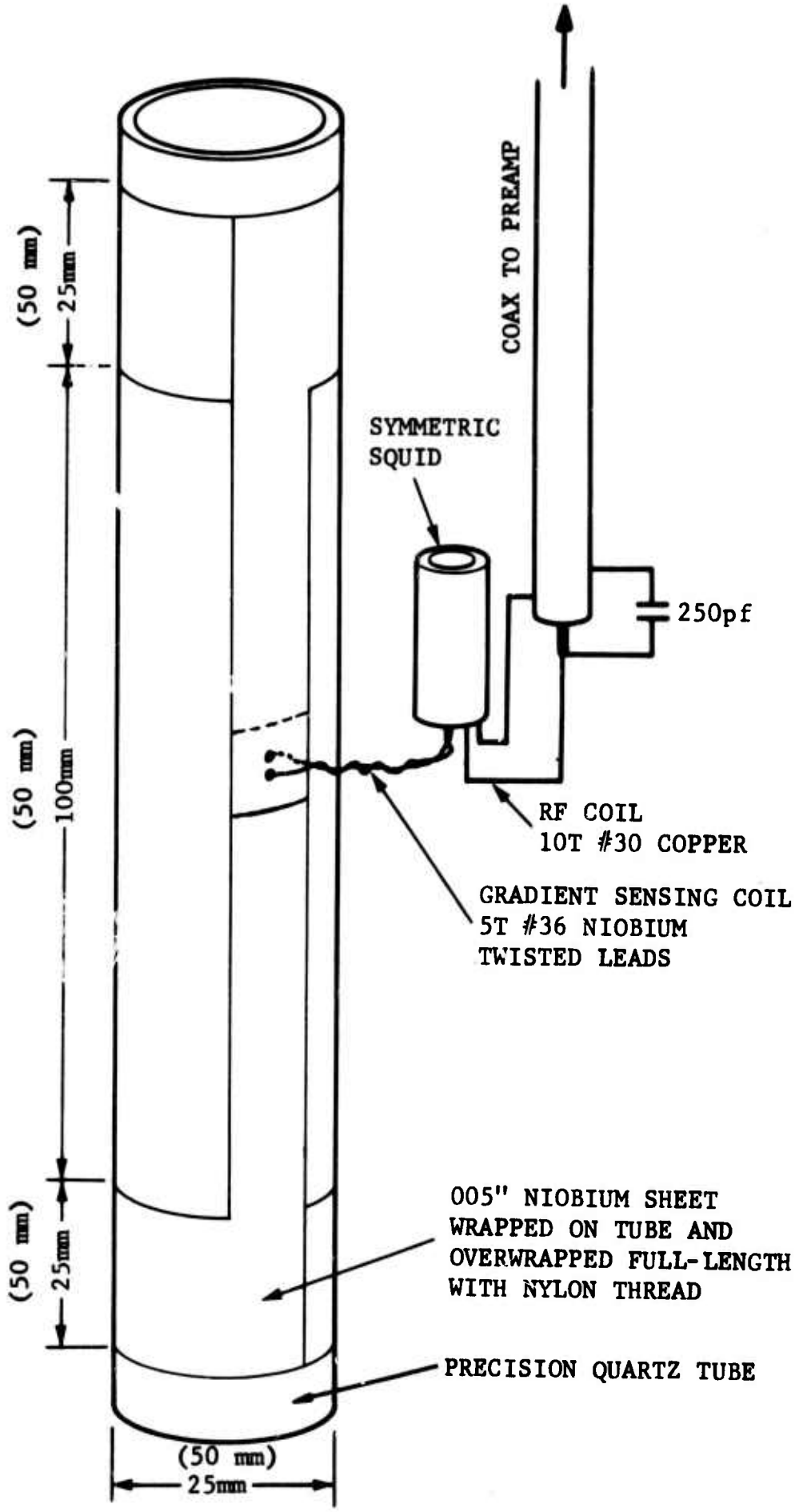

FIGURE 2-4. CONSTRUCTION OF GRADIENT-SENSITIVE FLUX TRANSFORMERS

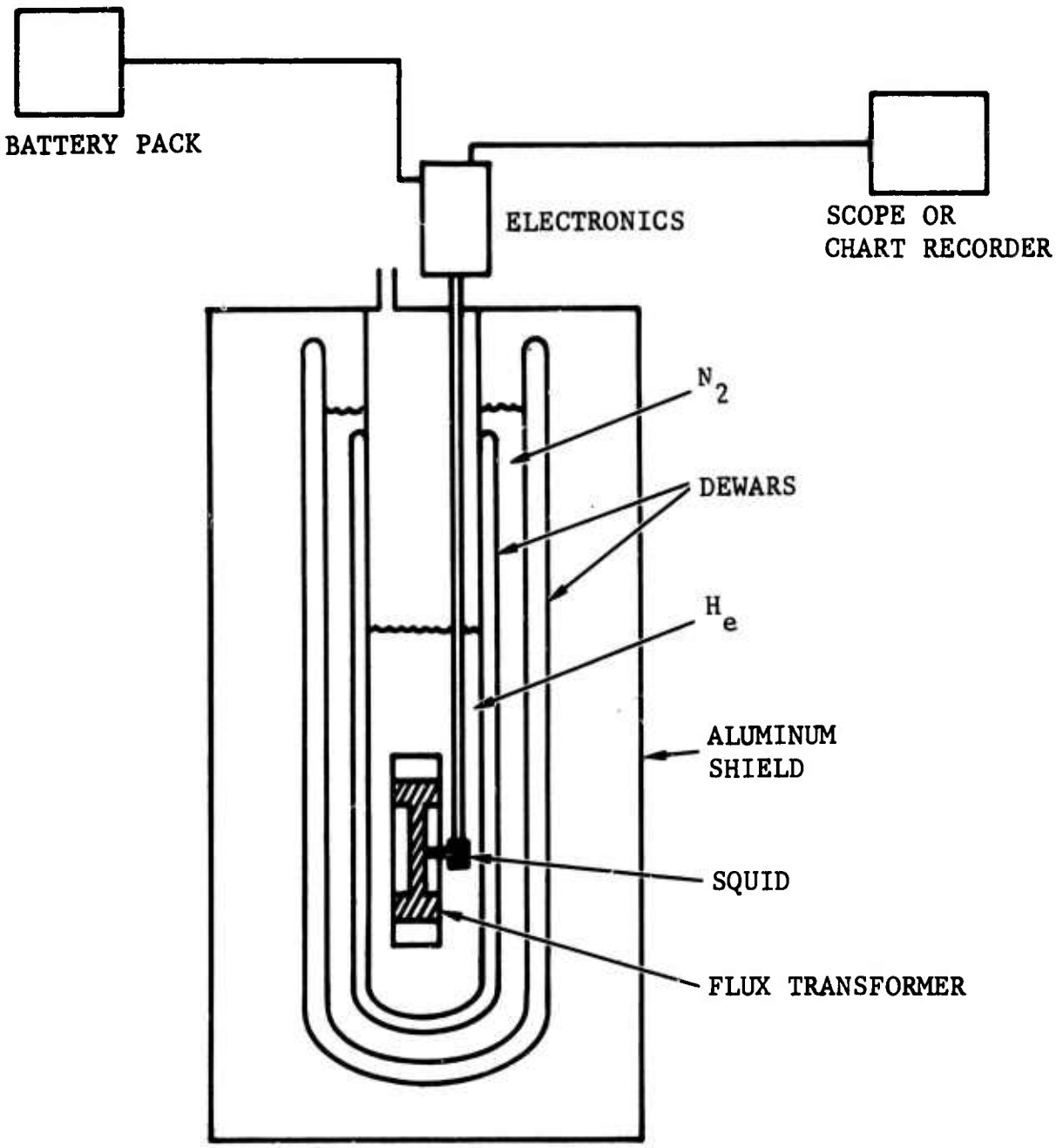

FIGURE 2-5. SIMPLIFIED PICTURE OF MAGNETIC GRADIOMETER AND CRYOSTAT. COMPENSATING CONTROL ELEMENTS NOT SHOWN

Figure 2-6 (this was Figure 9 of the Seventh Quarterly Technical Report No. U4717), that is, the rf oscillator, the audio oscillator, the pre-amplifier, the rf amplifier, the diode detector circuit, and also a gain-ten differential post-detection dc amplifier (not shown in the figure). These units were miniaturized and integrated into a package similar to the one shown in Figure 2-7.

At the time this first model was built, some important design principles, as discussed in the preceding section, had not been appreciated. First, the off-center mounting of the SQUID and the off-center flux-transformer interconnections (the vertical strips on the quartz tube) gave quite large response to transverse-field components, owing to the induced dipole moments of these diamagnetic objects. Second, the aluminum shield was displaced axially with respect to the flux transformer, and so fluctuations in the earth's field were seen by the flux transformer through the induced ac dipole moment of the shield.

In order to correct for the asymmetric mounting of the SQUID and flux transformer interconnections and other residual asymmetries, a set of three orthogonal control elements were introduced to null out the response to all three components of a uniform field. One element was a slug of 1/4" Nb mounted axially in the flux transformer and axially adjustable. The other two elements were rotatable Nb vanes mounted on the periphery of the glass tube. These are indicated schematically in Figure 2-8. All three control

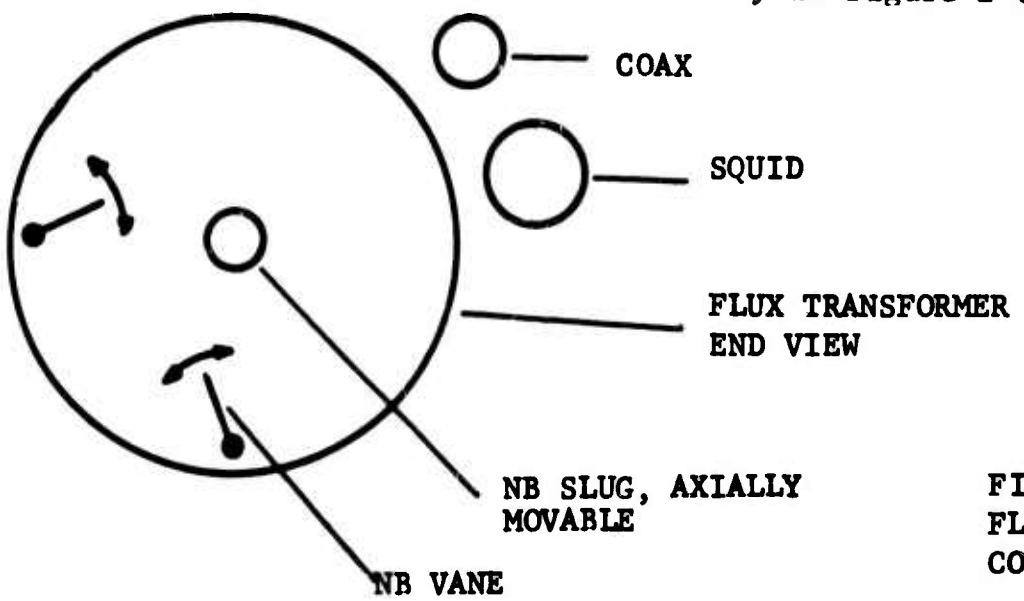

FIGURE 2-8. END VIEW OF FLUX TRANSFORMER SHOWING COMPENSATING ELEMENTS

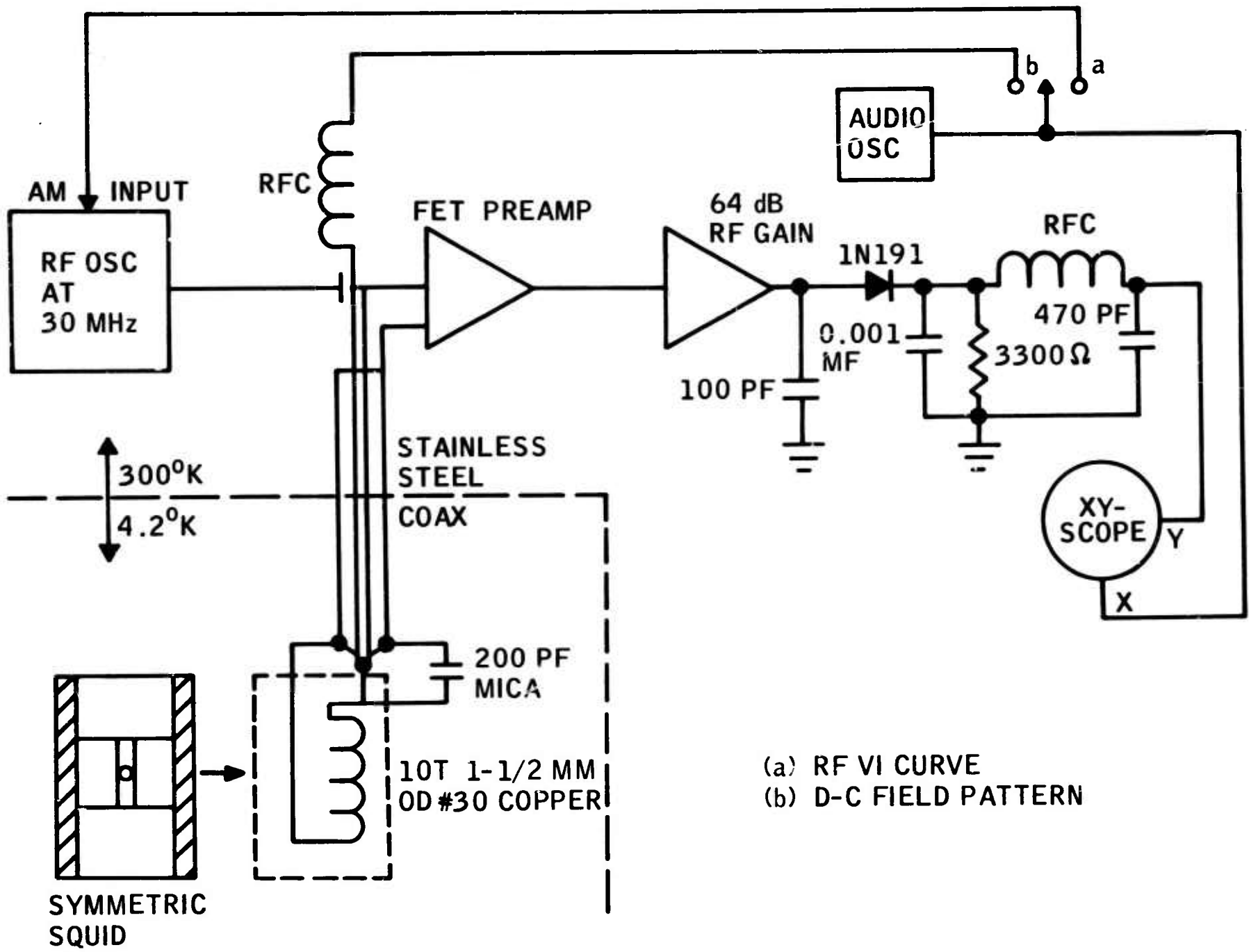

FIGURE 2-6. BLOCK DIAGRAM OF CRYOGENIC AND ELECTRONIC SYSTEM USED FOR MAGNETOMETRY

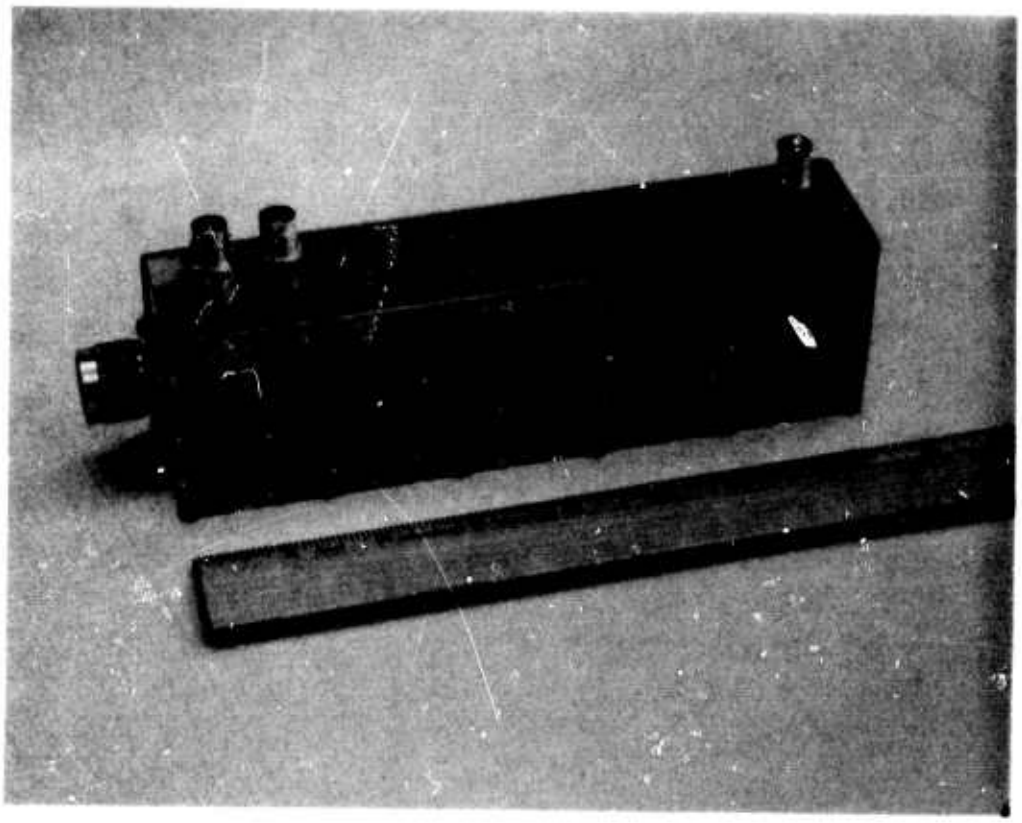

FIGURE 2-7. EXPERIMENTAL ELECTRONIC PACKAGE CONTAINING UNITS SHOWN IN FIGURE 2-6. TYPE N CONNECTOR TO COAX AT LEFT. OSCILLOSCOPE OR RECORDER OUTPUT BNC CONNECTOR AT RIGHT. OTHER CONNECTORS FOR BATTERY PACK AND TEST POINTS.

elements were operated by micarta rods passing through O-ring seals in the top of the cryostat.

Along with the addition of these control elements, the flux transformer itself was redesigned and made larger. The dimensions of the final experimental version are shown parenthetically in Figure 2-4.

As noted above, the aluminum shield was displaced axially with respect to the flux transformer, thus violating an essential design principle. For this reason, the final and most significant test of the redesigned gradiometer was made with the shield removed. In order that the SQUID not be swamped by radio signals and other interference, this test was made 450 feet underground, in the U. S. Borax Corporation mine at Boron, California (at a point in the mine designated by a marker as J1770).

Figure 2-9 shows a portion of the chart recording made during these tests, the recorder being connected in parallel with the oscilloscope indicated in Figure 2-6. The oscilloscope (a Sony-Tektronix battery-operated portable) was useful for seeing fast signals. The recorder averaging time was of the order of 1/2 second.

The earth's field gradient is said to be $\sim 10^{-7}$ gauss/ft or 3×10^{-9} gauss/cm. Therefore, drift in the accompanying record ($\sim 3 \times 10^{-8}$ g/cm in 5 minutes) clearly is not a change of the earth's field gradient, and is probably an instrumental effect caused by evaporation of N_2 and He with associated dimensional changes, or changes of the induced moment of the liquids themselves. The susceptibility of liquid He is of the order of 10^{-5}. Therefore, a changing helium level in the neighborhood of the upper loop of the transformer can produce a total field change of the order of 10^{-5} gauss, which is very much larger than the total range indicated in the record.

The pulse-type signals of $\sim$ 10 sec duration and $\sim 5 \times 10^{-9}$ gauss/cm amplitude clearly are non-random and might be associated with the operation of mine equipment (the period is about right) several hundred feet away,

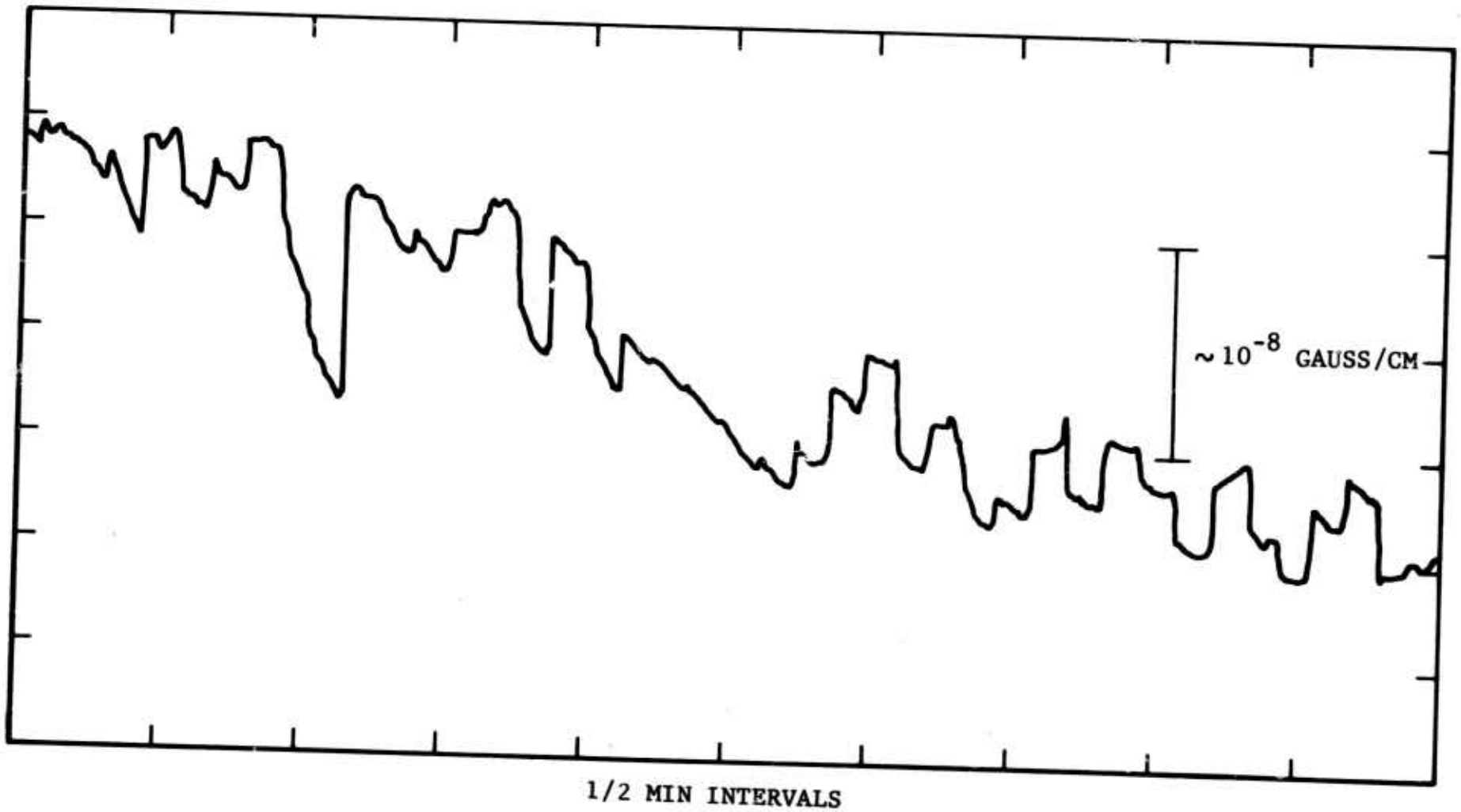

FIGURE 2-9. PORTION OF CHART RECORDING OF GRADIOMETER OUTPUT IN U. S. BORAX CORPORATION MINE TEST, DECEMBER 7, 1969.

but this has not been proved. It seems unlikely that such signals would be generated in the cryostat.

Mentally eliminating the drift and pulse signals, the remaining short-period fluctuations seem to be of the order of 10^{-10} gauss/cm. The ultimate sensitivity that one should achieve with a gradiometer with this geometry and dimensions (flux transformer loops 5 cm diameter on a 10 cm baseline) is less than 10^{-11} gauss/cm. This expected sensitivity can be calculated from the inherent noise level of the SQUID electronic system ($\sim \varphi_o/6000$, see Seventh Quarterly Technical Report, U-4717) along with the "coupling factor" F, defined as the ratio of flux applied to the transformer to the flux seen by the SQUID. The (previously measured) value of this ratio was 62, that is:

$$\frac{\varphi_{applied}}{\varphi_{SQUID}} = F = 62 . \qquad (2\text{-}19)$$

Therefore a noise level of $\varphi_o/6000$ at the SQUID is equivalent to a noise level of about $\varphi_o/100$ at the flux transformer. Since the transformer diameter was 50 mm, this is equivalent to an applied field fluctuation of

$$\delta B_z = (\varphi_o/100)\ (\frac{25\pi}{4}\ \text{cm}^2)^{-1} \cong 10^{-10}\ \text{gauss} ; \qquad (2\text{-}20)$$

or, since the gradiometer baseline $\ell \cong 10$ cm, to a gradient fluctuation of

$$\delta(\partial B_z/\partial_z) \cong 10^{-11}\ \text{gauss/cm}. \qquad (2\text{-}21)$$

During the course of the experiments at Boron, a 60 hz field of the order of $\varphi_o/10$ (i.e., far above the instrument noise level) was observed on the oscilloscope. This field came from mine equipment cables lying on the surface 450 feet above and within a few hundred feet horizontally. This allowed us to demonstrate in a dramatic way the design principle stated above, that normal conducting material (such as the aluminum shield) should be symmetrical with respect to the instrument. By simply placing a small sheet of aluminum, of the order of a few inches, alongside the

the instrument, the 60-cycle response was enhanced by a factor of 100 or more, owing to the induced ac dipole moment of the piece of aluminum.

To recapitulate, the short period fluctuations of $\sim 10^{-10}$ gauss/cm seen in the mine equipment is within a factor of ten of the ultimate sensitivity of 10^{-11} gauss/cm which one would predict (Eq. 2-21) for a gradiometer of this size. Also the instrumental drift was unacceptably large. Nevertheless, this and the preceding experiments clearly demonstrated the important design principles to be followed in gradiometer construction using superconducting sensors, so that one now knows how to build a practical operational instrument with the ultimate sensitivity. Also it should be emphasized that we have already reached sensitivity levels some orders of magnitude better than that of any currently available instrument.

2.6 MAGNETOCARDIOGRAPHY

A very interesting and potentially useful application of ultrasensitive magnetometers is in biological and medial studies. In particular, an appreciable ac field ($\sim 10^{-7}$ gauss peak) is associated with the human heartbeat. The cardiac field has been extensively investigated by David Cohen, using a 1,000,000-turn coil of copper wire as a sensor and a low-noise parametric amplifier. Such measurements require an extremely quiet magnetic environment, and Cohen has recently completed a triply magnetically shielded room for this purpose at the MIT Francis Bitter National Magnet Laboratory in Cambridge, Massachusetts. This facility provides ambient fields in the microgauss range, at an undetermined low noise level.

It seemed to be of considerable academic and practical interest to combine the superior sensitivity of a SQUID as a magnetometer with the superior magnetic environment provided by the Cohen facility, and to see what level of magnetic measurements might be possible and what the applications might be.

Two electronic units like that shown in Figure 2-7 were built, and two SQUID probes were adapted for purposes of the suggested experiment. One probe was a hermetically sealed type containing a C-shaped SQUID which had been built and adjusted in January 1968, and had since been used in numerous experiments and demonstrations for visiting firemen. The only adaptation required of this probe was a reduction of overall length to about 26 inches so that it would fit into an ordinary suitcase. The other probe contained one of the more elegant, and rugged, symmetric SQUID's. The two types of SQUID are shown in Figure 1-1. Since a symmetric SQUID is not by itself sensitive to uniform applied field, it was adapted to magnetometry by means of an exceedingly simple flux transformer made of 1/4 mm Nb wire, as sketched in Figure 2-10.

The experiments were carried out in the National Magnet Laboratory on the nights of December 29 and 30, using a glass helium Dewar borrowed from Dr. Maxwell. The probe extended into the tail section of the Dewar, which was about two inches O.D., so a human or other subject could get quite close to the actual sensor in the bottom end of the probe. Figure 2-11 shows the arrangement of Dewar and subject through the door of the shielded room. Figure 2-12 shows the electronic package, with cover removed, and the SQUID probe removed from the Dewar. Both probes gave very good results, the symmetric SQUID with the relatively large-aperture flux transformer giving the best signal-to-noise as expected. Figure 2-13 shows a human cardiac magnetic signal obtained with the superconducting sensor about 3 inches in front of the stomach. The peak signal is about 2 or 3 x 10^{-7} gauss. The upper trace is an electrocardiogram of the same subject taken a few hours later.

Although the two traces differ somewhat in detail, they show comparable signal-to-noise, so that magnetocardiography can now be regarded as a technique with significant possibilities for clinical and diagnostic use.

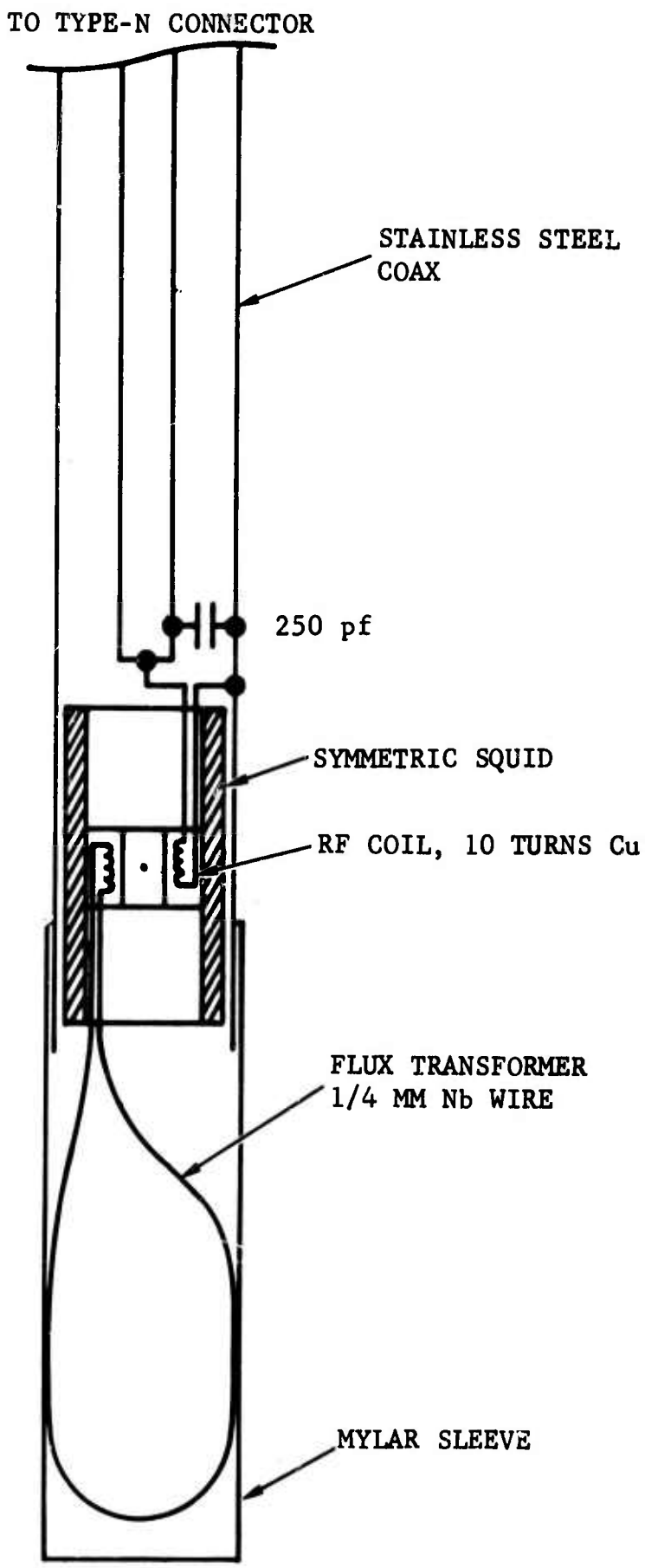

FIGURE 2-10. ARRANGEMENT OF SQUID AND FLUX TRANSFORMER IN LOWER END OF COAXIAL PROBE USED IN MAGNETOCARDIOGRAPHY.

FIGURE 2-11. VIEW THROUGH DOOR OF LOW-FIELD FACILITY IN FRANCIS BITTER NATIONAL MAGNET LABORATORY, SHOWING DEWAR MOUNT AND POSITION OF SUBJECT FOR MAGNETOCARDIOGRAM

FIGURE 2-12. SQUID ELECTRONIC PACKAGE (COVER REMOVED) AND COAXIAL PROBE. SYMMETRIC SQUID IN GIRL'S LEFT HAND.

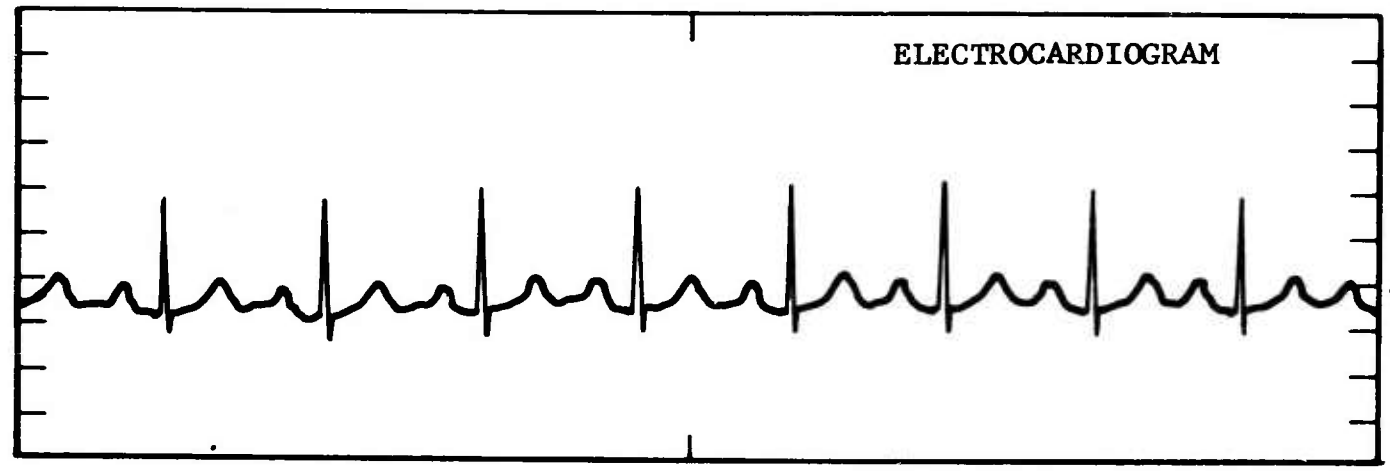

FIGURE 2-13. MAGNETOCARDIOGRAM OBTAINED WITH ARRANGEMENT OF FIGURE 11. ELECTROCARDIOGRAM OF SAME SUBJECT TAKEN A FEW HOURS LATER.

The background noise level indicated in the magnetocardiogram is considerably less than 10^{-8} gauss within the recorder bandpass of ~ 1 to 35 hz. Whether this noise originated in the superconducting sensing system (as suggested by Cohen), or in the shielded room (as hinted by the senior author of this report) remains to be determined. In any event, it is evident that the operational noise level of the total system is of the order of 10^{-9} gauss per $\sqrt{\text{hz}}$, which would seem to make it a rather potent system for the study of very low field phenomena.

SECTION 3

MATHEMATICAL ANALYSIS OF THE OPERATION OF QUANTUM-INTERFERENCE DEVICES

3.1 INTRODUCTION

The electronic system discussed in Section 2.5 is based upon the rudimentary circuit shown in Figure 3-1. The device is represented by the loop on the right. The voltage across the weak link is $V_2(t)$ and the current through the link is $I_2(t)$. It is assumed that the link is biased with a dc voltage V_o and has a quantum-phase difference θ_o across it due to the application of a dc magnetic field. The loop inductance is L_2.

The device is inductively coupled to the parallel-resonant circuit on the left. An rf current $I_1(t)$ is injected into the node of the resonant circuit, the voltage of which is $V_1(t)$.

In practical operation the device is commonly operated in the hysteretic mode, for which the critical current of the weak link I_c is not small with respect to $\bar{\varphi}_o/L_2$.* A simpler case to treat analytically, however, is that characterized by the condition $L_2 I_c \ll \bar{\varphi}_o$. In addition, we assume a simple, analytic relation between the link voltage and current; namely, the Josephson relation

---

* $\bar{\varphi}_o \equiv \varphi_o/2\pi$

$$I_2(t) = I_c \sin \frac{1}{\Phi_o} \int V_2(t)dt . \qquad (2\text{-}1)$$

The following heuristic treatment of this analytically more tractable, although less practical, case does provide some engineering insight into the proper choice of the circuit parameters.

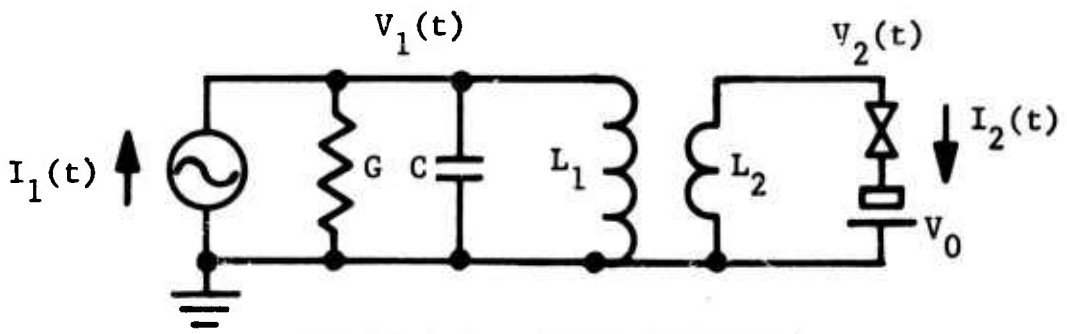

FIGURE 3-1. SQUID CIRCUIT

Assuming the Josephson relation (3-1), we find the nonlinear nodal equations of the network to be

$$Y(p)\, V_1(t) - \Gamma_{12}\, p^{-1}\, V_2(t) = I_1(t) \qquad (3\text{-}2)$$

and

$$-\Gamma_{12} p^{-1}\, V_1(t) + \Gamma_2 p^{-1}\, V_2(t) + I_c \sin \frac{1}{\Phi_o}\, p^{-1}(V_2(t) - V_o). \qquad (3\text{-}3)$$

In these equations $p \equiv d/dt$. The inverse inductances are $\Gamma_1 = [L_1(1 - k^2)]^{-1}$, $\Gamma_2 = [L_2(1 - k^2)]^{-1}$ and $\Gamma_{12} = k[\sqrt{L_1 L_2}(1 - k^2)]^{-1}$. The shorted-secondary admittance of the primary is $Y(p) = \Gamma_1 p^{-1} + Cp + G$.

Eliminating $V_2(t)$ from (3-3) by means of (3-2) yields a nonlinear equation for $V_1(t)$:

$$V_1(t) = Z(p)\, I_1(t) + \frac{\Gamma_{12}}{\Gamma_2} Z(p)\, I_c \sin\left\{\omega_o T + \theta_o - \frac{1}{\Gamma_{12}\bar{\varphi}_o}\left[Y(p)\, V_1(t) - I_1(t)\right]\right\}. \tag{3-4}$$

In expression (3-4) the primary impedance operator is

$$Z(p) = \Gamma_2 p/(\Gamma_2 p\, Y(p) - \Gamma_{12}^2) = \left(G + Cp + \frac{1}{L_1 p}\right)^{-1}.$$

The angular frequency of the Josephson oscillation is $\omega_o \equiv V_o/\bar{\varphi}_o$ and θ_o is the initial phase of the flux in the device loop.

3.2 JOSEPHSON OSCILLATOR

Perhaps the simplest application to be considered is that of the Josephson oscillator. In this case the weak link is voltage biased by V_o, the primary current generator $I_1(t)$ is absent, and the magnetic field applied to the device is zero, that is, $\theta_o = 0$. Under these conditions expression (3-4) reduces to

$$V_1(t) = \frac{\Gamma_{12}}{\Gamma_2} Z(p)\, I_c \sin\left[\omega_o t - \frac{Y(p)\, V_1(t)}{\Gamma_{12}\,\bar{\varphi}_o}\right]. \tag{3-5}$$

Because of the nonlinear nature of expression (3-5), $V_1(t)$ contains harmonics of ω_o. For present purposes it will be assumed that the parallel resonant circuit is tuned to ω_o and is of sufficiently high Q, so the only significant Fourier Bessel components in $V_1(t)$ are at $\pm\,\omega_o$.

Now, at resonance, that is, for $C = 1/\omega_o^2 L_1$, $Z(i\omega_o) = G^{-1} \mid 0$ and $Y(i\omega_o) \approx k^2/(1 - k^2)\omega_o L_1 \mid \underline{-\pi/2}$. This approximate expression for $Y(i\omega_o)$ holds if it is assumed that k is not too small: that is, if $[k^2/(1 - k^2)]^2 \gg (G\omega_o L_1)^2$.

Assuming the solution $V_1(t) = V_1 \sin(\omega_o t - \alpha)$ for (3-5) we find then

$$V_1 \sin(\omega_o t - \alpha) = k\sqrt{\frac{L_2}{L_1}}\frac{1}{G} I_c \left\{ J_o\left(\frac{1}{k}\sqrt{\frac{L_2}{L_1}}\frac{V_1}{V_o}\right) \sin \omega_o t + \right.$$

$$\left. J_2\left(\frac{1}{k}\sqrt{\frac{L_2}{L_1}}\frac{V_1}{V_o}\right) \sin\left[\omega_o t - 2(\omega_o t - \alpha - \frac{\pi}{2})\right]\right. \qquad (3\text{-}6)$$

It follows that $\alpha = 0$ and

$$V_1 = k\sqrt{\frac{L_2}{L_1}}\frac{1}{G} I_c \left\{ J_o\left(\frac{1}{k}\sqrt{\frac{L_2}{L_1}}\frac{V_1}{V_o}\right) + J_2\left(\frac{1}{k}\sqrt{\frac{L_2}{L_1}}\frac{V_1}{V_o}\right)\right.$$

$$= 2k^2 \frac{V_o}{V_1}\frac{1}{G} I_c J_1\left(\frac{1}{k}\sqrt{\frac{L_2}{L_1}}\frac{V_1}{V_o}\right) . \qquad (3\text{-}7)$$

The corresponding average power delivered to G is

$$P = \frac{1}{2} G V_1^2 = k^2 V_o I_c J_1\left(\frac{1}{k}\sqrt{\frac{L_2}{L_1}}\frac{V_1}{V_o}\right) . \qquad (3\text{-}8)$$

The first and largest maximum of J_1 occurs when the argument is ~ 1.8, at which value $J_1 \approx 0.58$. Thus, the maximum power is delivered to G when, according to (3-8),

$$G = 0.36 \frac{L_2}{L_1}\frac{I_c}{V_o} . \qquad (3\text{-}9)$$

The maximum power is then

$$P_{max} = 0.58\, k^2 V_o I_c . \qquad (3\text{-}10)$$

The assumption made above with respect to k not being too small now becomes

$$\left[k^2/(1 - k^2)\right]^2 >> (0.36\, L_2 I_c/\bar{\varphi}_o)^2 . \qquad (3\text{-}11)$$

3.3 RF-BIASED MAGNETOMETER

The next application of considerable interest is magnetometry. In this case the phase θ_o is simply the total magnetic flux in the device loop divided by $\bar{\varphi}_o$ and the voltage bias is zero.

As a first approximation for $V_1(t)$ it is reasonable to take $V_1(t) = Z(p)\, I(t)$. According to (3-4) the next approximation is

$$V_1(t) = Z(p)\left\{I_1(t) + \frac{\Gamma_{12}}{\Gamma_2} I_c \sin\left[\theta_o - \frac{Y(p)\, Z(p) - 1}{\Gamma_{12}\, \bar{\varphi}_o} I_1(t)\right]\right\} . \tag{3-12}$$

Again, the resonant circuit is assumed to have a high Q and tuned so that the only significant Fourier-Bessel components in $V_1(t)$ are at $\pm\omega$.

Choosing the excitation current to be $I_1(t) = I \sin \omega t$, we find that (3-12) reduces to

$$V_1(t) = Z\Big\{I \sin(\omega t - \beta) + 2k\sqrt{\frac{L_2}{L_1}} I_c J_1\Big(k\sqrt{\frac{L_2}{L_1}} \frac{1}{\bar{\varphi}_o} \frac{ZI}{\omega}\Big) \cos\theta_o \sin\Big(\omega t - 2\beta - \frac{\pi}{2}\Big)\Big\} \tag{3-13}$$

where $Z(i\omega) = Z \angle -\beta$.

Expression (3-13) can be alternatively written

$$V_1(t) = \text{Imag}\, Z\Big\{1 + 2K\sqrt{\frac{L_2}{L_1}} \frac{I_c}{I} J_1\Big(k\sqrt{\frac{L_2}{L_1}} \frac{ZI}{\bar{\varphi}_o \omega}\Big) \cos\theta_o\, e^{-i(\beta + \frac{\pi}{2})}\Big\} Ie^{i(\omega t - \beta)} \tag{3-14}$$

It is convenient to define a complex amplitude function A such that

$$V_1(t) = \text{Imag } \hat{A}\, Ie^{i(\omega t - \beta)}.$$

We find from (3-14) the magnitude of $\hat{A}$ to be

$$|\hat{A}| \approx Z\left\{1 - 2k\sqrt{\frac{L_2}{L_1}}\frac{I_c}{I} J_1\left(k\sqrt{\frac{L_2}{L_1}}\frac{ZI}{\bar{\varphi}_o\omega}\right)\cos\theta_o \sin\beta\right\}, \qquad (3\text{-}15)$$

if $$\left(2k\sqrt{\frac{L_2}{L_1}}\, I_c/I\right)^2 \ll 1.$$

The effect of varying the applied magnetic field, that is, of changing θ_o, is evidently maximum when the excitation is adjusted to $k\sqrt{\frac{L_2}{L_1}}\frac{ZI}{\bar{\varphi}_o\omega} = 1.8$, for which value J_1 is maximum and equal to 0.58. When this condition obtains, the sensitivity of the amplitude function to change in the magnetic field is

$$\frac{\partial|\hat{A}|}{\partial\theta_o} \approx 2k^2 \frac{L_2}{L_1}\frac{Z\, I_c}{\bar{\varphi}_o\omega} Z \sin\beta \sin\theta_o . \qquad (3\text{-}16)$$

This sensitivity function (3-16) is zero when the circuit is tuned to resonance, that is, when it is tuned to $\beta = 0$. It is maximum when the circuit is detuned to $\beta = \pm\pi/4$, or to $Z \sin\beta = \pm 1/2G$. When the circuit is so adjusted.

$$\frac{\partial|\hat{A}|}{\partial\theta_o} \approx \pm\frac{1}{\sqrt{2}} k^2 \frac{L_2}{L_1}\frac{I_c}{G^2\bar{\varphi}_o\omega} \sin\theta_o \qquad (3\text{-}17)$$

is the sensitivity of the magnetometer. The periodic variation of rf impedance with dc magnetic fields discussed in Section 1-4 is explicit in result (3-17).

SECTION 4

CONCLUDING REMARKS

During the course of this work, a large number of experiments with superconducting small-area contacts have been performed. These experiments resulted in the development of some practical devices, the application of the devices as electromagnetic sensors both at very low and at very high frequencies, and a detailed understanding of how the devices work, particularly vis-a-vis thermal fluctuations and environmental noise.

Actually not all of the work has been reviewed or presented in this final report. Rather complete and detailed accounts are given in some of the earlier technical reports, in particular the 1968 Final Technical Report, dated November 15, 1968, and in the Fifth, Sixth, and Seventh Quarterly Technical Reports, dated respectively March 7, 1969, June 15, 1969, and September 15, 1969. Also, a series of three papers is to appear very shortly in the Journal of Applied Physics, probably in the February 1970 issue. These are entitled, "Design and Operation of Stable Rf-Biased Superconducting Point-Contact Quantum Devices, and a Note on the Properties of Perfectly Clean Metal Contacts," by J. E. Zimmerman, Paul Thiene, and J. T. Harding; "Quantum Phase Fluctuations in Resistive Circuits Containing Weakly Superconducting Junctions," by J. T. Harding

and J. E. Zimmerman, and "Heterodyne Detection with Superconducting Point Contacts, and Enhanced Heterodyne Signals from Tightly-Coupled Contacts," by J. E. Zimmerman. One paper was published earlier, entitled "Quantum Interference Magnetometry and Thermal Noise from a Conducting Environment," by J. T. Harding and J. E. Zimmerman, in Physics Letters Vol. 27A, p 670 (1968). Another paper is to be submitted for publication shortly, on the subject of magnetocardiography using superconducting sensors, by David Cohen and J. E. Zimmerman. A number of papers have been presented orally at technical conferences on work done under this contract.

During the last few months, the senior author of this report has collaborated with A. H. Silver on the preparation of a review article entitled, "Josephson and Weak-Link Devices," to appear in a Treatise on Applied Superconductivity, edited by Vernon Newhouse and published by Academic Press. While the scope of this article is broader than the work done under this contract, the author has nevertheless drawn heavily on knowledge and experience acquired during the term of the contract. Consequently, the review article will reveal much of the philosophy which has guided this work.

REFERENCES

Bean, C. P., DeBlois, R. W., and Nesbitt, L. B., J. Appl. Phys. 30, 1976 (1959).

Cohen, D., J. Appl. Phys. 40, 1046 (1969).

Cohen, D., Symposium on Application of Magnetism in Bioengineering, to be published in the IEEE Transactions on Magnetism, summer of 1970.

Dayem, A. H. and Grime, C. C., Appl. Phys. Letters 9, 47 (1966).

Eck, R. E., Scalapino, D. J., and Taylor, B. N., Proc. LT9 Part A, p 415, Plenum Press (1965).

Harding, J. R. and Zimmerman, J. E., Phys. Letters 27A, 670 (1968).

Harding, J. T. and Zimmerman, J. E., in press for J. Appl. Phys., February 1970.

Kamper, R. A., Symposium on the Physics of Superconducting Devices, sponsored by ONR. University of Virginia, Charlottesville (1966).

Lambe, J., Silver, A., Jaklevic, R., and Mercereau, J., Physics Letters 11, 16 (1964).

Silver, A. H. and Zimmerman, J. E., Phys. Rev. 158, 423 (1967).

Silver, A. H., Zimmerman, J. E., and Kamper, R. A., Appl. Phys. Letters 11, 209 (1967).

Silver, A. H. and Zimmerman, J. E., Treatise on Applied Superconductivity, edited by V. L. Newhouse (to be published by Academic Press).

Vant Hull, L., Simpkins, R., and Harding, J. T., Phys. Letters 24, 736 (1967).

Zimmerman, J. E., RSI 32, 502 (1961).

Zimmerman, J. R., Cowan, J. A., and Silver, A. H., Appl. Phys. Letters 9, 353 (1966).

Zimmerman, J. E. and Silver, A. H., J. Appl. Phys. 39, 2679 (1968).

Zimmerman, J. E., Thiene, P., and Harding, J. T., in press for J. Appl. Phys., February 1970.

Zimmerman, J. E., in press for J. Appl. Phys., February 1970.

ACKNOWLEDGEMENTS

The work described in this and previous reports was carried out mainly by Dr. John Harding, Mr. Wayne Leicht, Dr. Paul Thiene, and Dr. James Zimmerman. In the early stages of the work, worthwhile contributions were made by Mr. Gordon McCone, Mr. Lynn Simpkins and Mr. Victor Hoover. Many useful discussions were held with members of the Ford Scientific Laboratory: Dr. M. Nisenoff, Dr. L. Vant Hull, Dr. Robert Eck, Dr. Harris Notaries, and Mr. Edward Helm among others. We also profited from discussions with Prof. John Wheatley of UCSD, Prof. R. Burgess of the University of British Columbia and Dr. Arnold Silver of the Aerospace Corporation. Last, but not least, we are very grateful for the stimulating interest and helpful suggestions of Mr. Edgar Edelsack of the Office of Naval Research.

Unclassified
Security Classification

DOCUMENT CONTROL DATA - R&D

(Security classification of title, body of abstract and indexing annotation must be entered when the overall report is classified)

1. ORIGINATING ACTIVITY *(Corporate author)*
Philco-Ford Corporation
Aeronutronic Division
Ford Road, Newport Beach, Calif. 92663

2a. REPORT SECURITY CLASSIFICATION
Unclassified

2b GROUP

3. REPORT TITLE
Quantum-Interferometer Device and Application Development

4. DESCRIPTIVE NOTES *(Type of report and inclusive dates)*
Final Technical Report II - 15 October 1968 to 15 December 1969

5. AUTHOR(S) *(Last name, first name, initial)*
Zimmerman, James E.
Thiene, Paul

6. REPORT DATE	7a. TOTAL NO. OF PAGES	7b. NO. OF REFS
January 16, 1970	57	18

8a. CONTRACT OR GRANT NO.
N00014-68-C-0138

b. PROJECT NO.
ARPA 1049, Modification No. P001

c.

d.

9a. ORIGINATOR'S REPORT NUMBER(S)
U4779

9b. OTHER REPORT NO(S) *(Any other numbers that may be assigned this report)*

10. AVAILABILITY/LIMITATION NOTICES

11. SUPPLEMENTARY NOTES

12. SPONSORING MILITARY ACTIVITY
Office of Naval Research
Physics Branch, Main Navy Building
Washington, D.C. 20360

13. ABSTRACT

This is a report on work done over a two-year period, from October 1967 to January 1970, on the development and applications of superconducting quantum devices, and the limitations imposed by thermal and environmental noise. Several types of stable point-contact niobium devices were developed for use as uhf heterodyne detectors, millimeter-wave video detectors, uhf mixers, vlf detectors, magnetometers, and for a number of other uses. As magnetometers these devices provide sensitivities as high as 10^{-9} gauss in compact, portable instruments. With such an instrument magnetocardiography has been put on a level comparable to electrocardiography. Experiments with a terrestrial magnetic gradiometer demonstrate the possibility of achieving gradient sensitivities of $\sim 10^{-10}$ gauss/cm for magnetic anomaly detection, and it is likely that subsequent developments will realize sensitivities at least one or two orders of magnitude better than this.

DD FORM 1 JAN 64 1473

Unclassified
Security Classification